Supporting Information

Engineering Au/Cu Interfaces to Promote *CO Spillover for High C_{2+} Selectivity in CO_2 Electroreduction

Fangmu Wang[1,#], Hao Tian[2,#], Gen Chen[1], Zhen Zhao[1], Wenguang Tu[2],wei Jiang[1,] and Guigao Liu[1,*]*

[1]School of Chemistry and Chemical Engineering, Nanjing University of Science and Technology, Nanjing, Jiangsu 210094, China

[2]School of Science and Engineering, The Chinese University of Hong Kong, Shenzhen 518172, China

*E-mail: jiangwei_nssperc@njust.edu.cn; guigao.liu@njust.edu.cn

[#]These authors contribute equally to this work.

Experimental procedures

Materials

Copper chloride dihydrate ($CuCl_2 \cdot 2H_2O$, purity>99.7%), sodium hydroxide (NaOH, 98%), polyvinyl pyrrolidone (PVP, M=58000), and potassium bicarbonate ($KHCO_3$, 99.5%) were purchased from aladdin Co., Ltd. L-Ascorbic acid was purchased from Acros Organics Co., Ltd. Chloroauric acid ($HAuCl_4$, 48-50% for Au), potassium hydroxide (KOH, 98%) and Ethanol were purchased from Sinopharm Chemical Reagent Co., Ltd. Deuterium oxide (D_2O, 99.9%) was purchased from Meryer (Shanghai) Biochemical Technology Co., Ltd. Nafion 212 cation exchange membrane was purchased from Alfa Aesar China Co., Ltd.

Preparation of $Cu_2O(100)$

Typically, 4 mmol of $CuCl_2 \cdot 2H_2O$ was added to 400 mL of deionized water and magnetically stirred at 55 °C for 30 minutes. Subsequently, 80 mmol of NaOH was dissolved in 40 mL deionized water and added dropwise to the $CuCl_2$ solution under continuous stirring. After 30 minutes, 24 mmol of ascorbic acid dissolved in 40 mL deionized water was added dropwise to the above mixture solution. After reaction for 3 hours at 55 °C under continuous stirring, $Cu_2O(100)$ was collected and washed in water and ethanol, and finally dried under vacuum at 60 °C for 12 h.

Preparation of $Cu_2O(111)$

Typically, 4 mmol of $CuCl_2 \cdot 2H_2O$ and 17.69 g of PVP were added to 400 mL of deionized water and magnetically stirred at 55 °C for 30 minutes. Subsequently, 80 mmol of NaOH dissolved in 40 mL deionized water was added dropwise to the above solution under

continuous stirring. After 30 minutes, 24 mmol of ascorbic acid dissolved in 40 mL deionized water was added dropwise to the above mixture solution. After reaction for 3 hours at 55 °C under continuous stirring, $Cu_2O(111)$ was collected and washed in water and ethanol, and finally dried under vacuum at 60 °C for 12 h.

Preparation of Au@$Cu_2O(100)$ or Au@$Cu_2O(111)$

100 mg of $Cu_2O(100)$ or $Cu_2O(111)$ was added to 15 mL of water to form a suspension solution under ultrasonic treatment, followed by the addition of 100 μL of 1 wt% $HAuCl_4$ aqueous solution under vigorous magnetic stirring. Then, the mixture solution was subjected to the light irradiation under a Xenon lamp for 60 minutes at room temperature. After being washed thoroughly in water and ethanol, the product was collected and dried under vacuum at 60 °C for 12 h.

Material characterization

The morphology characterization was performed using a JSM-7800F PRIME scanning electron microscope (SEM). Transmission electron microscopy (TEM) characterization, including high-resolution TEM (HRTEM) imaging and energy-dispersive X-ray spectroscopy (EDS) mapping, was carried out on a JEM-F200 transmission electron microscope. X-ray diffraction (XRD) patterns were collected on a Bruker D8 Advance diffractometer. Surface chemical property of the samples was investigated by X-ray photoelectron spectroscopy (XPS) on a Thermo Scientific K-Alpha spectrometer. The loadings of Au were determined using inductively coupled plasma optical emission spectrometry (ICP-OES) on a Thermo Fisher Scientific iCAP PRO spectrometer.

Electrocatalytic CO_2 reduction (ECO_2RR)

For the preparation of the working electrode, 8 mg of catalyst was dispersed in a mixed solvent consisting of 10 μL of 5 wt% Nafion solution and 990 μL of ethanol. The suspension was subjected to ultrasonication for 30 minutes. Subsequently, 3.4 mg cm^{-2} of the catalyst ink was drop-cast onto a glassy carbon electrode (GCE) with a diameter of 6 mm. An Ag/AgCl electrode and a platinum electrode were employed as the reference and counter electrodes, respectively.

ECO_2RR tests were conducted in an H-type liquid cell using a Corrtest CS350M electrochemical workstation. 0.1 M $KHCO_3$ aqueous solution was used as the electrolyte. Prior to ECO_2RR measurements, the cathodic electrolyte was purged with CO_2 gas at 20 mL min^{-1} for 30 minutes. All potentials were measured against the Ag/AgCl reference electrode and converted to the reversible hydrogen electrode (RHE) scale using the equation:

$$E_{RHE} = E_{Ag/AgCl} + 0.223 + 0.059 \times pH \quad (1)$$

For the ECO_2RR measurement in the flow cell, a platinum foil, , a gas diffusion electrode (GDE) loaded with the catalyst, and an Hg/HgO electrode were used as counter, working and reference electrodes. A Fumasep FAB-PK-130 anion-exchange membrane was used to separate the cathode and the anode. The catalyst ink was prepared by dispersing 20 mg of catalyst in a mixture solution containing 3 mL ethanol, 30 μL of 5 wt% Nafion solution, and 10 μL of 2 wt% PTFE emulsion. The catalyst loading is1 mg cm^{-2} on the GDE electrode. The anolyte and catholyte compartments were both filled with 1.0 M KOH

electrolyte. The anolyte was circulated at 120 mL min^{-1} using a gas-liquid mixed flow pump, while the catholyte was delivered at 40 mL min^{-1} via a peristaltic pump. Concurrently, CO_2 was introduced into the cathodic compartment at 20 mL min^{-1}.

Gaseous products were analyzed using a gas chromatography (Shimadzu GC-2014). Liquid products were measured by a nuclear magnetic resonance (NMR) spectroscopy (Bruker AVANCE NEO 500 MHz). In the NMR measurements, DMSO was used as internal standard.

The Faradaic efficiency (FE) of products was calculated by the equation:

$$FE = \frac{zFn}{Q} * 100 \quad (2)$$

Where z represents the number of electrons transferred for product formation, n is the mole of product, F is Faraday constant (96485 C/mol), and the Q is the amount of cumulative charge recorded by the electrochemical workstation.

Operando **attenuated total reflection surface-enhanced infrared absorption spectroscopy (ATR-SEIRAS) measurements**

The electrochemical measurements were performed within a custom-designed cell configuration. The working electrode comprised a silicon-based attenuated total reflectance (ATR) crystal coated with a thin gold film, onto which the catalyst was uniformly deposited at a mass loading of 1 mg cm^{-2}. An Ag/AgCl electrode and a platinum wire served as the reference and counter electrodes, respectively. This cell was seamlessly coupled to a Bruker INVENIO-S spectrometer, equipped with a liquid nitrogen-cooled

mercury cadmium telluride (MCT) detector. *Operando* infrared spectra were acquired across a range of applied potentials to monitor surface species evolution during electrochemical operation.

Operando Raman measurements

The *Operando* Raman measurements were conducted using a Gaoss union flow cell coupled with a Renishaw inVia Raman spectrometer. A carbon paper loaded with catalyst served as the working electrode, while a Hg/HgO reference electrode and a platinum wire counter electrode were employed. 0.1 M $KHCO_3$ aqueous solution was used as the electrolyte, which was circulated through both cathode and anode chambers at a flow rate of 10 mL min^{-1} using a peristaltic pump. Raman spectra were collected with a 785 nm excitation laser.

Calculation details

The adsorption, diffusion, and transformation of CO were investigated by using density functional theory (DFT) calculations with a 520 eV cutoff for the plane-wave basis set. The projected augmented wave method was employed as implemented in the Vienna Ab-initio Simulation Package to represent nuclei and core electrons.[1, 2] The electron exchange-correlation was described by using the revised Perdew-Burke-Ernzerhof (RPBE) form of the generalized gradient approximation (GGA).[3, 4] The van der Waals interactions were estimated with the D3 semiempirical approach of Grimme with the Becke-Johnson (BJ) damping function[5]. A (2,2,1) k-point sampling was used for all calculations. Transition states were calculated using the climbing image nudged elastic band (NEB) method, with

forces converged to 0.04eV/Å[6]. To build the Au-Cu interface, a (6 × 6) supercell of either Cu(111) or Cu(100) slab with four atomic layers was adopted as the substrate where the bottom layer was fixed to simulate the bulk, and an Au_{30} and Au_{20} cluster was respectively added on the top of Cu(100) and Cu(111). To simulate the solvent environment, a single layer of either five (for Cu(100)) or seven (for Cu(111)) water molecules at the surface.

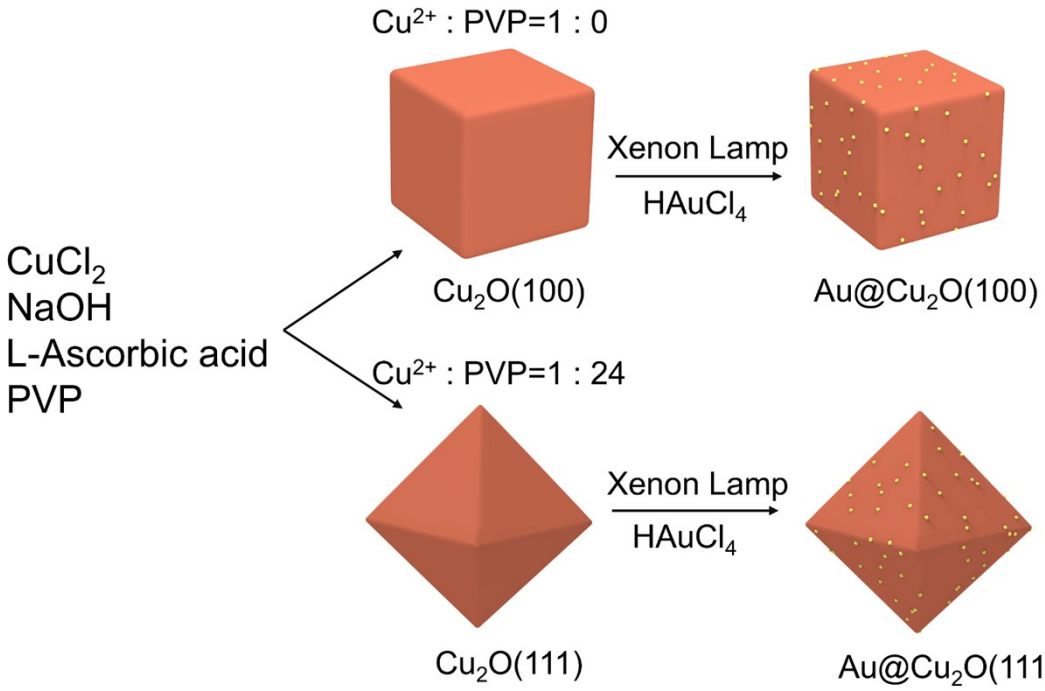

Figure S1. Schematic diagram of illustrating the synthesis of $Cu_2O(100)$, Au@ $Cu_2O(100)$, $Cu_2O(111)$ and $Au@Cu_2O(111)$.

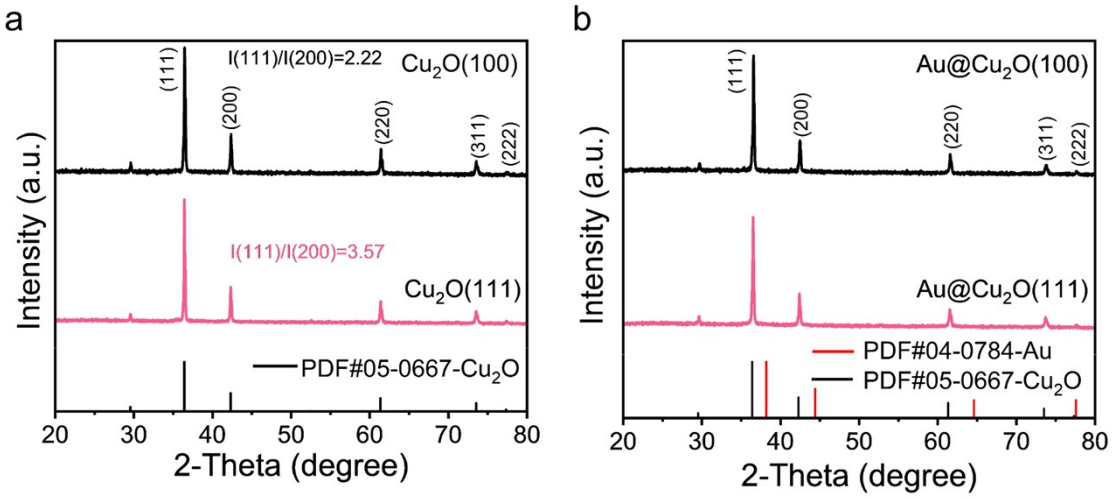

Figure S2. XRD patterns of (a) $Cu_2O(100)$ and $Cu_2O(111)$, (b) $Au@Cu_2O(100)$ and $Au@Cu_2O(111)$.

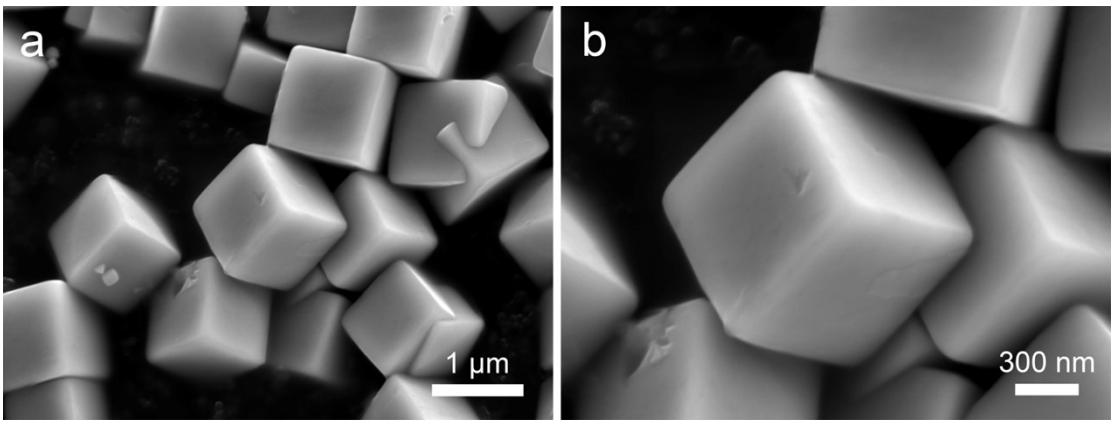

Figure S3. SEM images of $Cu_2O(100)$ in (a) low and (b) high magnifications.

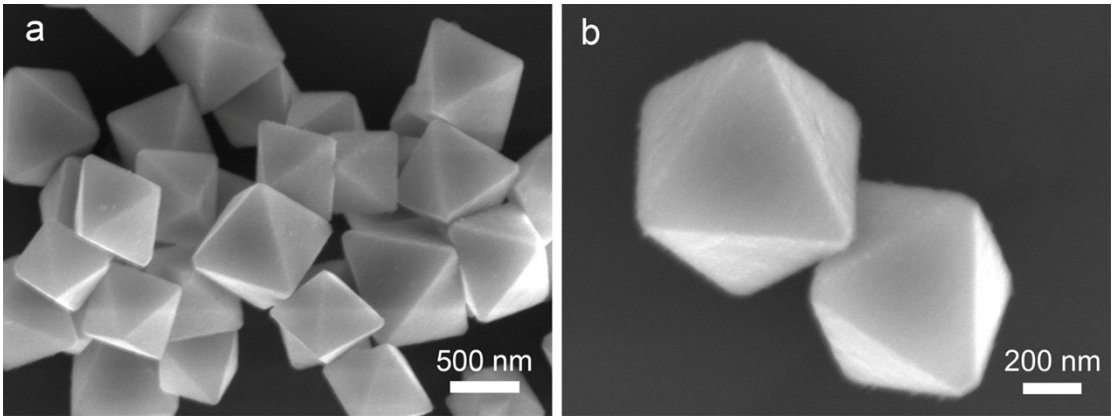

Figure S4. SEM images of $Cu_2O(111)$ in (a) low and (b) high magnifications.

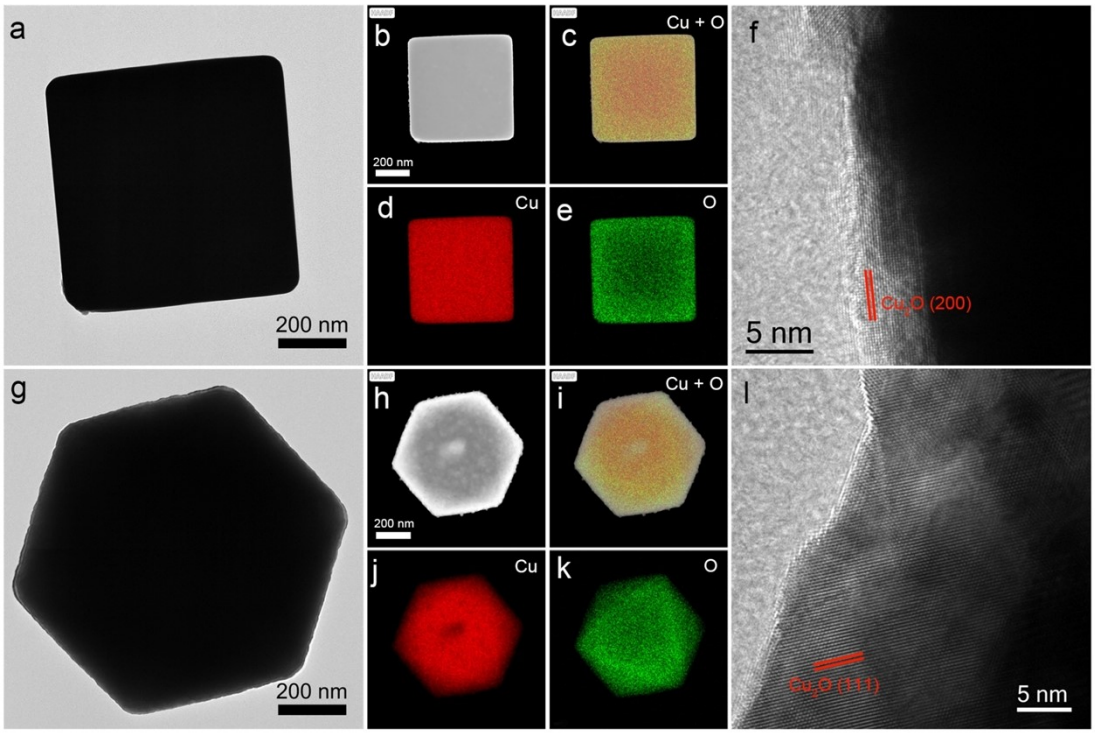

Figure S5. (a) TEM, (b-e) EDS element mapping, and (f) HRTEM images of $Cu_2O(100)$. (g) TEM, (h-k) EDS element mapping, and (l) HRTEM images of $Cu_2O(111)$.

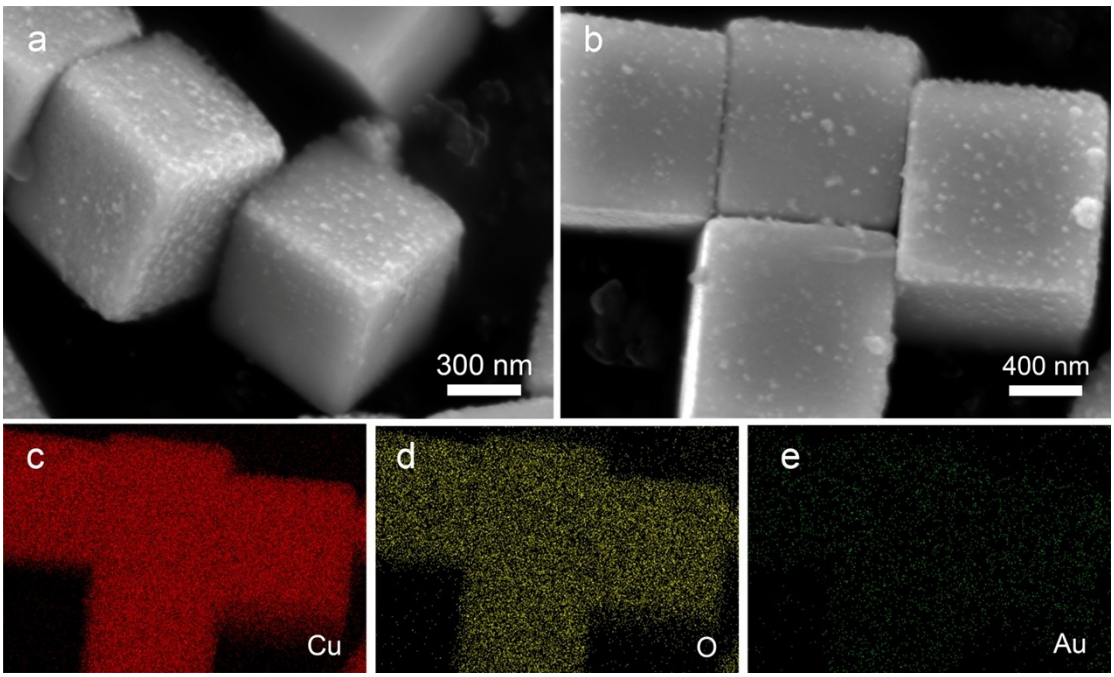

Figure S6. (a, b) SEM, and (c-e) EDS elemental mapping images of Au@Cu_2O(100).

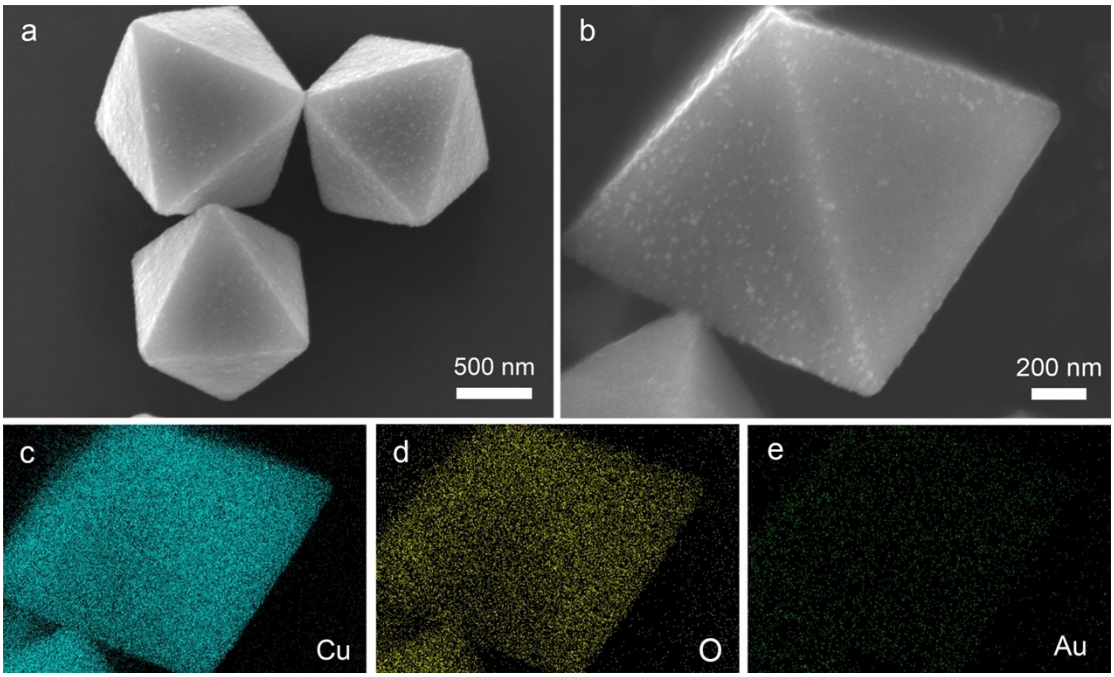

Figure S7. (a, b) SEM, and (c-e) EDS elemental mapping images of Au@Cu_2O(111).

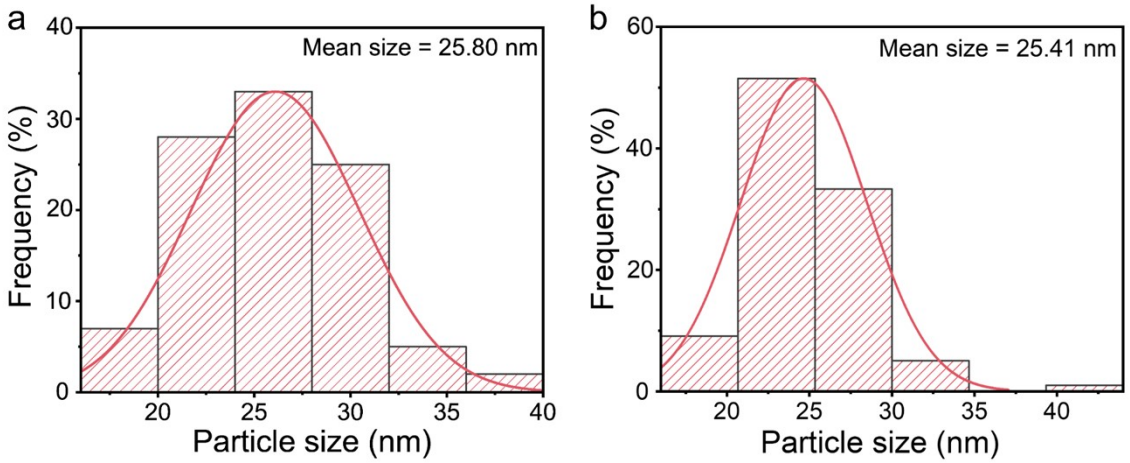

Figure S8. The histogram of size distribution of Au nanoparticles for (a) Au@Cu_2O(100) and (b) Au@Cu_2O(111).

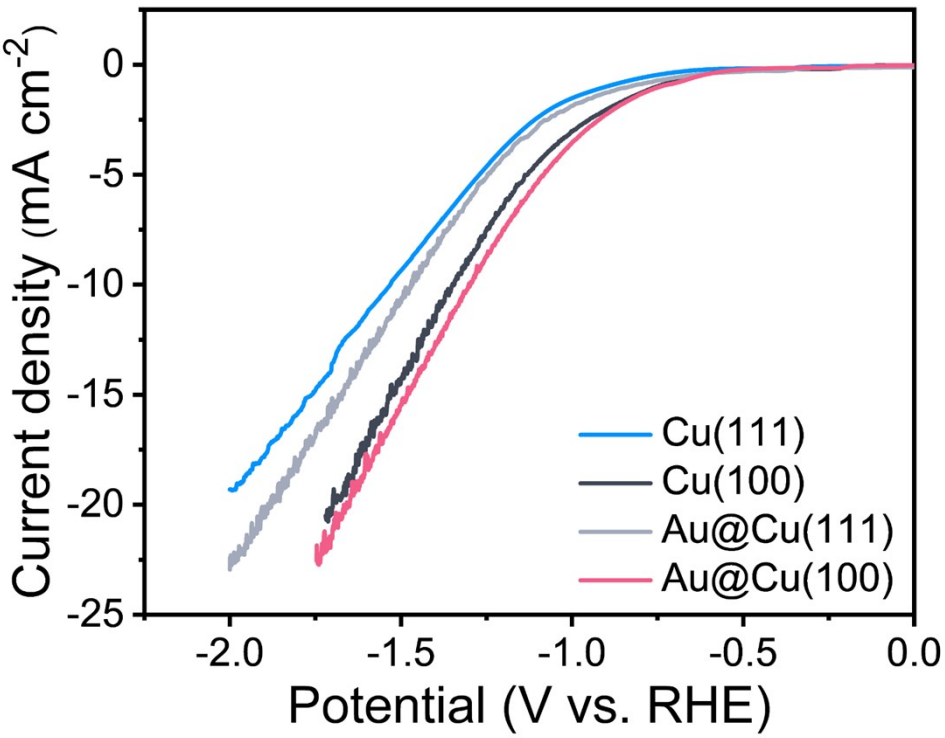

Figure S9. LSV curves of Cu(111), Cu(100), Au@Cu(111) and Au@Cu(100) measured in CO_2-saturated 0.1 M $KHCO_3$ solution.

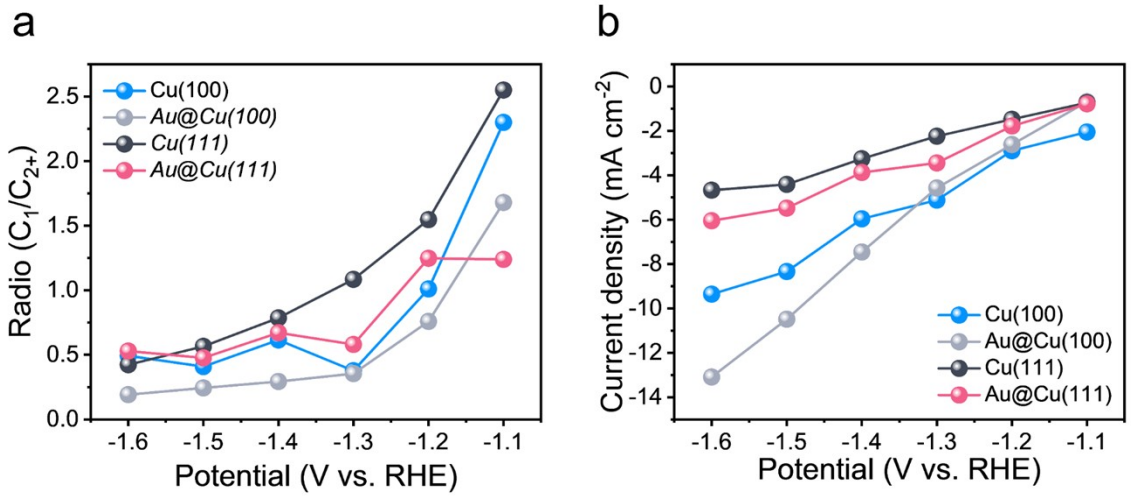

Figure S10. (a) Ratio of C_1 to C_{2+} for Cu(100), Au@Cu(100), Cu(111) and Au@Cu(111) measured at various potentials. (b) Partial current densities of C_{2+} products for Cu(100), Au@Cu(100), Cu(111) and Au@Cu(111).

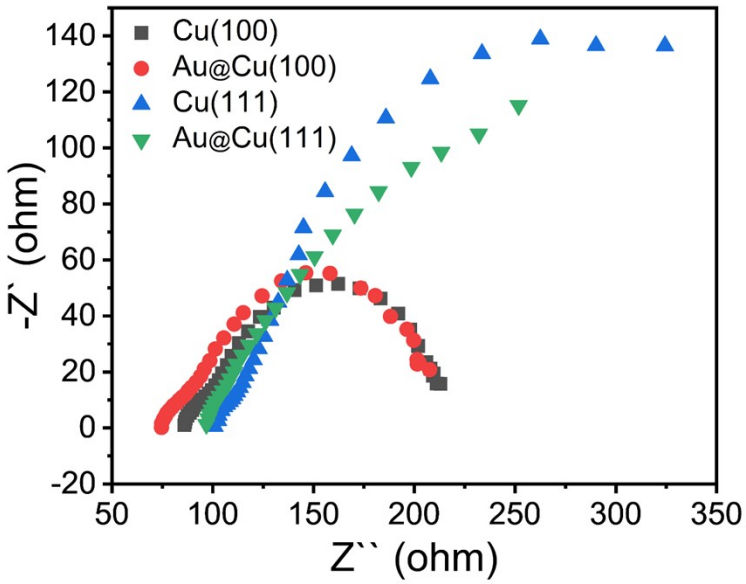

Figure S11. EIS spectra of Cu(100), Au@Cu(100), Cu(111) and Au@Cu(111) measured in CO_2-saturated 0.1 M $KHCO_3$ solution.

.

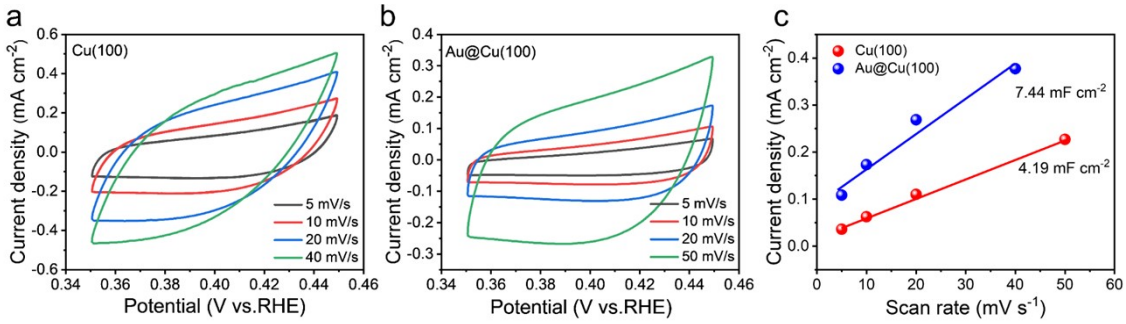

Figure S12. Electric double layer capacitance (C_{dl}) measurements at the non-Faradaic region (from −0.35 to −0.45 V vs. RHE) over (a) Cu(100) and (b) Au@Cu(100). (c) Charging current density differences plotted against the scan rates over Cu(100) and Au@Cu(100).

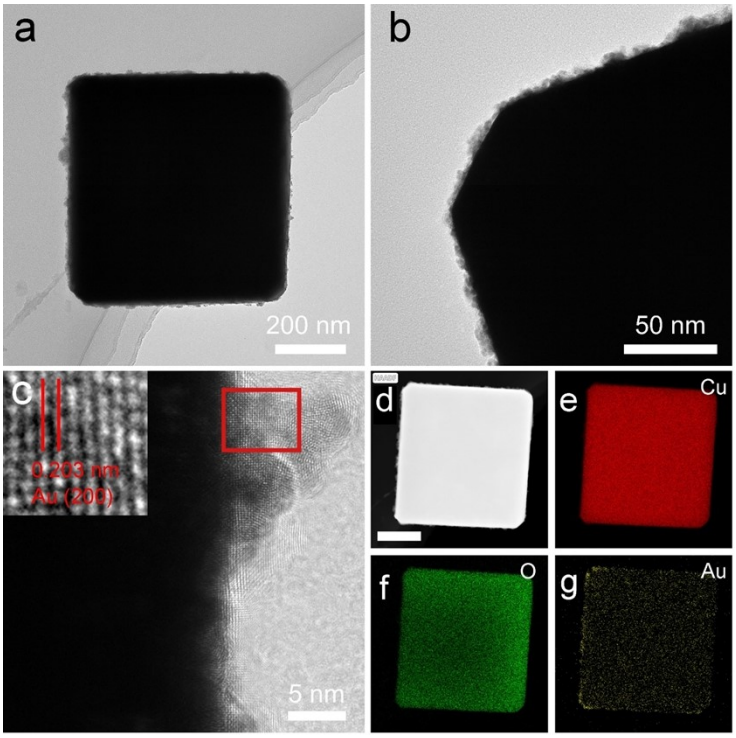

Figure S13. (a, b) TEM, (c) HRTEM, and (d-g) EDS element mapping images of Au@Cu(100) taken after the stability test at −1.5 V vs. RHE. The scale bar in (d) is 200 nm.

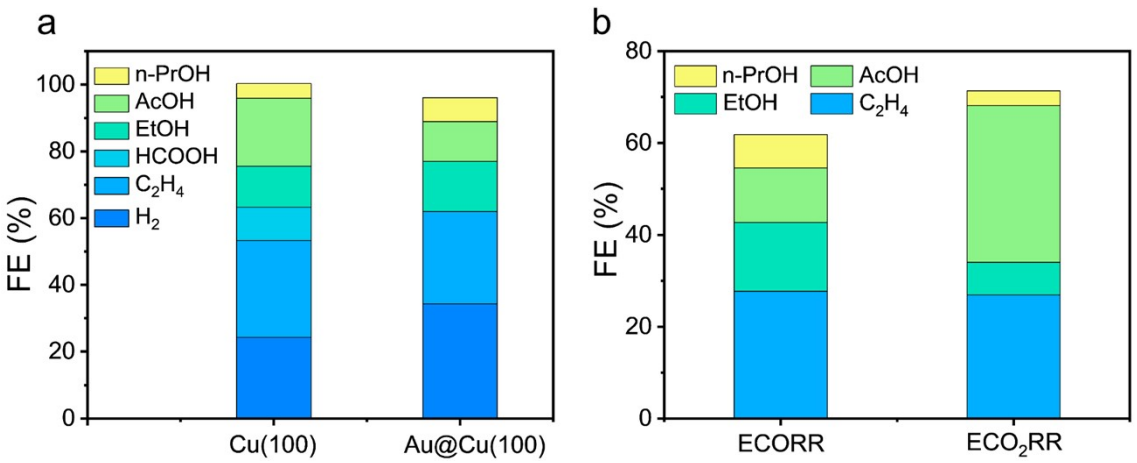

Figure S14. (a) Product distributions of Cu(100) and Au@Cu(100) under ECORR. (b) Product distributions of Au@Cu(100) under ECORR and ECO_2RR.

Table S1. Compositions of Au@Cu(100) and Au@Cu(111) measured by ICP-OES.

Samples	Au (wt%)	Cu (wt%)
Au@Cu_2O(100)	0.40	66.5
Au@Cu_2O(111)	0.41	66.4

Table S2. Comparison of the ECO_2RR performance of Au@Cu(100) catalyst with that of some recently reported state-of-the-art Cu-based tandem electrocatalysts.

Electrocatalysts	**C_{2+} FE (%)**	**C_{2+} partial current density (mA cm^{-2})**	**Stability (h)**	**References**
Au@Cu(100)	**71**	**−400**	**12**	**This work**
L-0.5-Au@OD-Cu	66	−300	/	7
Cu-Au NCAs	43.2	−8.47	24	8
Au-Cu Janus NSs	67	−290	12	9
Cu_{cub}-Ag	54.8	/	/	10
a-Ni/Cu-NP@CMK	72.3	−406.1	15	11
NP $Ag_{58}Cu_{18}$	73	−30	3.3	12
Ag-Cu 5 %	80.2	−320	60	13
Ni SAC+Cu-R	62	−500	14	14
EP-CoP/Cu	76.8	−726	25	15
PTF(Ni)/Cu	57.3	−3.5	11	16

References

1. P. E. Blöchl, *Phys. Rev. B*, 1994, **50**, 17953-17979.
2. G. Kresse and J. Furthmüller, *Comput. Mater. Sci.*, 1996, **6**, 15-50.
3. J. P. Perdew, K. Burke and M. Ernzerhof, *Phys. Rev. Lett.* , 1996, **77**, 3865-3868.
4. B. Hammer, L. B. Hansen and J. K. Nørskov, *Phys. Rev. B*, 1999, **59**, 7413-7421.
5. S. Grimme, J. Antony, S. Ehrlich and H. Krieg, *J. Chem. Phys.*, 2010, **132**.
6. G. Mills, H. Jónsson and G. K. Schenter, *Surf. Sci.*, 1995, **324**, 305-337.
7. S. Wang, H. D. Jung, H. Choi, J. Kim, S. Back and J. Oh, *Nano Energy*, 2024, **130**, 110176.
8. Y. Yan, H. Zhou, T. Li, D. Wang, P. Schaaf, G. Guo and X. Wang, *Small*, 2026, **22**, 2501125.
9. Y. Zheng, J. Zhang, Z. Ma, G. Zhang, H. Zhang, X. Fu, Y. Ma, F. Liu, M. Liu and H. Huang, *Small*, 2022, **18**, 2201695.
10. P. Iyengar, M. J. Kolb, J. R. Pankhurst, F. Calle-Vallejo and R. Buonsanti, *ACS Catal.*, 2021, **11**, 4456-4463.
11. B. Chen, L. Gong, N. Li, H. Pan, Y. Liu, K. Wang and J. Jiang, *Adv. Funct. Mater.*, 2024, **34**, 2310029.
12. H. Pan, J. Wu, X. Lu, Y. Li, Q. Zhang, J. Ling, Y. Wang and B. Min, *ACS Appl. Energy Mater.*, 2025, **8**, 8299-8310.
13. Z. Cai, N. Cao, F. Zhang, X. Lv, K. Wang, Y. He, Y. Shi, H. Bin Wu and P. Xie, *Appl. Catal. B-Environ.*, 2023, **325**, 122310.
14. M. Liu, Q. Wang, T. Luo, M. Herran, X. Cao, W. Liao, L. Zhu, H. Li, A. Stefancu, Y.-R. Lu, T.-S. Chan, E. Pensa, C. Ma, S. Zhang, R. Xiao and E. Cortés, *J. Am. Chem. Soc.*, 2024, **146**, 468-475.
15. C. Wang, Y. Sun, Y. Chen, Y. Zhang, L. Yue, L. Han, L. Zhao, X. Zhu and D. Zhan, *Adv. Sci.*, 2024, **11**, 2404053.

16. D.-L. Meng, M.-D. Zhang, D.-H. Si, M.-J. Mao, Y. Hou, Y.-B. Huang and R. Cao, *Angew. Chem. Int. Ed.*, 2021, **133**, 25689-25696.